PROCEEDINGS OF ECOS 2023 - THE 36TH INTERNATIONAL CONFERENCE ON
EFFICIENCY, COST, OPTIMIZATION, SIMULATION AND ENVIRONMENTAL IMPACT OF ENERGY SYSTEMS
25-30 JUNE 2023, LAS PALMAS DE GRAN CANARIA, SPAIN

Techno-Economic Optimization of an Innovative Plant for Sustainable Iron Reduction

Elisa Corbean[a], Jannik Neumann[b], Frank Dammel[b], Peter Stephan[b], Stefan Ulbrich[a]

[a] Department of Mathematics, Technical University of Darmstadt, Darmstadt, Germany,
{corbean, ulbrich}@mathematik.tu-darmstadt.de
[b] Institute for Technical Thermodynamics, Technical University of Darmstadt, Darmstadt, Germany,
{neumann, dammel, pstephan}@ttd.tu-darmstadt.de

Abstract:
Metal fuels such as iron represent potential energy carriers for large-scale storage and transport of renewable energy. In a circular process renewable energies can be stored in form of iron by thermochemical reduction of iron oxide and the required energy can be released via thermochemical oxidation, time and location independent from the storage process. While existing infrastructure such as coal-fired power plants could be retrofitted to meet the needs for the oxidation process, the conceptualization and construction of new infrastructure for the storage process by reduction is required. This opens up the possibility for a thorough techno-economic assessment of potential processes in order to ensure the optimal process design. Therefore, a techno-economic model of an innovative reduction plant utilizing the flash ironmaking technology for the reduction reactor is developed. The resulting mathematical model describes the operation of the reduction plant in dependence of design variables defining the plant components' dimensions. These design variables together with further process variables are optimized using mathematical optimization with respect to an economic objective function, i.e. the levelized cost of iron, in order to obtain the economically optimal process design. Thorough analyses are performed to assess the impact of changing economic boundary conditions on the optimal process design. Numerical results demonstrate a strong dependence of the cost optimal design on the available renewable energy prices and the obtained levelized cost of iron varies between 0.05 $/kg iron and 0.68 $/kg iron. Thus, choosing appropriate reduction locations with access to low renewable energy prices is crucial for the economic competitiveness of the considered process. The results further confirm an expected trade-off between total investment costs and yearly energy consumption of the plant components. With increasing cost for renewable energy, energetically more efficient system designs also become economically advantageous, i.e. an increase in the energetic efficiency from η_{sys} = 55.6% to η_{sys} = 69.3% is observable. The electrolyzer turns out to be the dominant plant component both, economically and energetically. Future work will take uncertainties into account to ensure a robust process design and couple the reduction plant to location specific renewable energy systems.

Keywords:
Iron as Energy Carrier; Mathematical Optimization; Metal Fuels; Process Design.

1. Introduction

While the ongoing energy crisis sets various challenges, it also acts as an accelerator for the global renewable capacity expansion [1]. Thus, the role of renewable energies (REs) becomes even more important in the endeavor to tackle climate change. However, the potential for RE is not equally distributed around the globe and their availability is subject to fluctuations over time. This turns the efficient global use of REs into a challenge especially for countries with low RE potential.
Suitable carbon-neutral energy carriers could remedy the situation by allowing long-term storage and secure transport of energy from RE sources. This way the energy carrier could be charged with energy from RE sources in locations with high RE potential, transported to locations with low RE potential, but high demand and the energy could be further stored on-site or released according to current demands.
Metal fuels are currently under investigation [2–4] as candidates for such energy carriers due to their high volumetric energy density [3] and their advantageous storage and transport properties. Especially iron seems to be a promising alternative to hydrogen as RE energy carrier [2, 5].
Using iron as an energy carrier, RE can be stored at sites with high RE potential via the thermochemical reduction of iron oxide with green hydrogen to produce iron. The resulting iron can then be transported to regions where energy is required and released via an oxidation reaction through combustion with air. The produced iron oxide is recycled and can again be charged from RE sources (cf. Fig. 1) leading to a circular

https://doi.org/10.52202/069564-0117

energy economy.
While the retrofit of coal-fired power plants for the iron combustion proves to be a promising way for making use of already existing infrastructure and assets [4, 6], the need for developing cost and energy efficient infrastructure at the reduction sites persists. Therefore, this work focuses on an optimal process design for an innovative plant reducing iron oxide to iron using green hydrogen obtained from RE sources.
The considered reduction plant uses a flash ironmaking reactor, which is described in [7] and found to be advantageous with respect to the size and energy requirements compared to common shaft furnace reduction plants. Figure 2 depicts the considered plant with all associated components including the water electrolysis for the production of green hydrogen. The goal of this work is to find an optimal process design for the assessed plant with respect to techno-economic objectives.

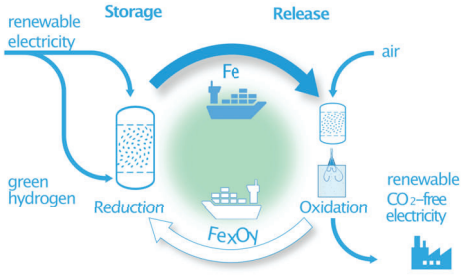

Figure 1: The iron energy cycle

Table 1: Design variables of the process components

Component	Design variable	Unit
Flash Reactor	Volume V	m^3
Air Heater Iron Oxide Preheater Hydrogen Preheater Condenser	Area A	m^2
Air Fan Recycle Compressor Electrolyzer	Electric power P_{el}	MW

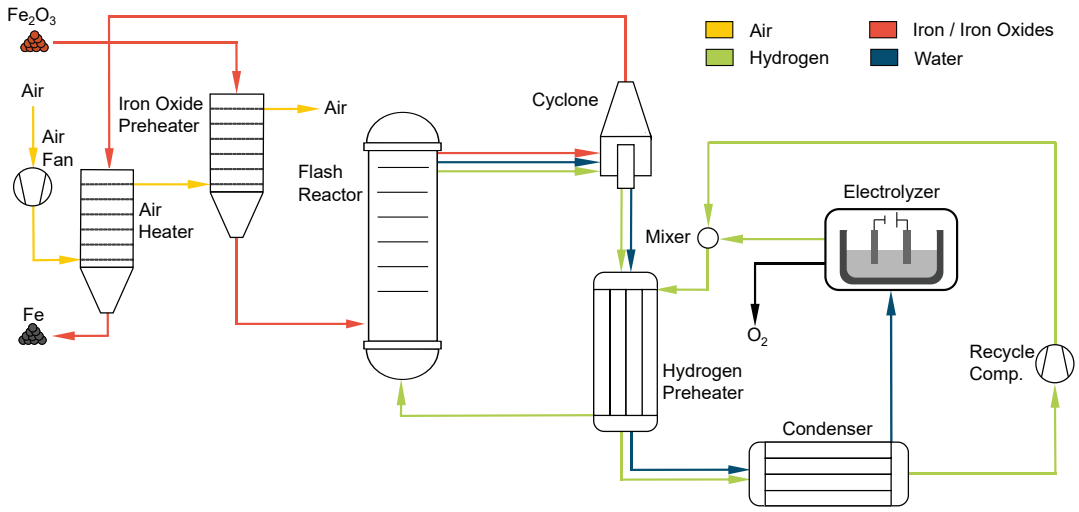

Figure 2: Components of an innovative plant for thermochemical reduction of iron oxides to iron

2. Process description

Blast furnace-based ironmaking remains dominant for steel production, but a more sustainable approach is emerging with the shaft furnace reduction method. Unlike blast furnaces that use coal as a reduction agent, shaft furnaces can reduce CO_2 emissions by utilizing natural gas or green hydrogen. While pure hydrogen-based shaft furnace direct reduction on a large scale has not yet been achieved, it has been technically proven feasible. However, iron oxide pellets are required as feedstock, and must be processed further into iron powder for the oxidation. An alternative technology is the flash ironmaking process [8, 9], which directly utilizes fine iron ore particles without additional pre-treatment, eliminating the need for pelletization and powder production. The flash reactor reduction technology is a high-intensity process that operates at high temperatures, unlike other gas-based ironmaking processes (shaft furnaces or fluidized-bed reactors). To attain these temperatures, the hydrogen reduction of iron oxide requires an external heat source. This heat can be generated internally by burning a portion of the reducing agent.
The reduction process depicted in Fig. 2 starts with fine iron oxide powder, the product of the previous oxidation, which is preheated in a bulk solid heat exchanger (iron oxide preheater). Subsequently, it is fed into the flash reactor where it reacts with a preheated hydrogen stream, yielding iron and water (R1). Heat is supplied

https://doi.org/10.52202/069564-0117

to the reactor, to sustain this endothermic reaction. The reactor effluent is then separated through a cyclone, with the hot iron being cooled down by a bulk solid heat exchanger (air heater) that uses the available heat to preheat the iron oxide feed via heat transfer to a secondary fluid (air). The hot gaseous reaction products (water and unreacted hydrogen) leaving the cyclone are used in a regenerative heat exchanger (hydrogen preheater) to preheat the gaseous reactants and the majority of the water is condensed out in the condenser. The remaining hydrogen is then recycled and merged with hydrogen produced by the electrolyzer, before being fed to the hydrogen preheater and finally entering the flash reactor.

The conversion of iron oxides (Fe_2O_3) to iron (Fe) and water (H_2O) through reduction with hydrogen (H_2) is described by the global reaction (R1). However, it is actually a step wise reaction sequence that involves intermediate iron oxides other than hematite (Fe_2O_3) [10]. These intermediate steps are not taken into account in accordance with the later-used kinetic model [8]. Furthermore, excess hydrogen, which is quantified with a hydrogen equivalence ratio λ_{H_2}, is required due to thermodynamic equilibrium limitations [8, 10] that may inhibit the full conversion.

$$Fe_2O_3 + 3\,\lambda_{H_2} H_2 \longrightarrow 2\,Fe + 3\,\lambda_{H_2} H_2O + 3\,(\lambda_{H_2}\text{-}1)\,H_2 \qquad \Delta H_r(\lambda_{H_2} = 1) = 98.77\,\mathrm{J\,mol^{-1}} \tag{R1}$$

The reaction is modelled on the basis of a global nucleation and growth rate equation for the overall reduction processes derived by Chen et al. [8]:

$$\frac{dX}{dt} = 4.41 \cdot 10^7 e^{\frac{-E_A}{R \cdot T}} \cdot \left(p_{H_2} - \frac{p_{H_2O}}{K_{eq}}\right) \cdot (1 - X), \tag{1}$$

where X is the fractional reduction degree, R is the universal gas constant, T the reaction temperature in K, $E_A = 214\,000\,\mathrm{J/mol}$ the activation energy of the reaction, p_s corresponds to the partial pressures in atm and K_{eq} to the equilibrium constant. From the rate law it becomes clear that the presence of water negatively affects the reduction by lowering the partial pressure of hydrogen but also decreases the thermodynamic reducing power of the gas due to the equilibrium limitations. This can have further implications on the whole process, since the gaseous effluent should be recycled and in ideal case purified into pure hydrogen to inhibit the negative impact. The kinetic law was derived based on hematite particles with an average size of 20 µm and a temperature range between 1423 K-1623 K [8]. This temperature range is used as variable bound for the reactor temperature during the optimization process to assure its correct operation.

3. Mathematical model

Detailed process analyses are crucial in the development of new technologies. Thermodynamic feasibility studies and energetic assessments offer valuable insights into the energetic efficiency of new processes. However, to evaluate the potential profitability and competitiveness of new processes, techno-economic considerations must also be taken into account. Therefore, a techno-economic assessment of the previously described reduction process is performed by directly applying mathematical optimization. This requires an explicit mathematical process description which is then used to obtain the cost optimal design of the system components for varying conditions (i.e. price for RE) by applying mathematical optimization algorithms to an economic objective function. Thus, a cost optimal design refers to a process design minimizing the economic objective, in this case the levelized cost of iron.

Every module in the reduction plant is modelled via incoming and outgoing mass flow rates $\dot{m}_{in,s}$ and $\dot{m}_{out,s}$ associated with species s, temperatures T_{in} and T_{out}, system pressures p_{in} and p_{out} as well as further component specific variables. Appropriate variable bounds on these process variables (e.g. reactor temperature) assure the correct operation of the modules. The underlying processes of each module are then described in terms of (in)equality constraints, including mass, species, and energy balances, as well as pressure changes and equations specific to individual components. The formulation of these technological constraints is closely linked to the cost functions of the equipment, which results in a complex nonlinear interplay between the employed thermodynamic and economic models.

3.1. Design variables

Since the optimization objective aims at finding the cost optimal process design, the functionalities of the modules are described in dependence on design variables, which are summarized in Table 1, responsible for the dimensioning of the modules.

In the case of the heat exchangers and the condenser, their respective area A together with the heat transfer coefficient U, the maximum temperature difference ΔT_{max} and the minimum temperature difference ΔT_{min} determines the heat flow $\dot{Q}_{therm}$ transferred from the hot flow to the cold flow [11]:

$$\dot{Q}_{therm} = \frac{\Delta T_{max} - \Delta T_{min}}{\ln\left(\frac{\Delta T_{max}}{\Delta T_{min}}\right)} \cdot U \cdot A. \tag{2}$$

https://doi.org/10.52202/069564-0117

For compressors, the necessary electric power P_{el} for obtaining an output pressure of p_{out} is determined in dependence of the inlet pressure p_{in}, temperature T_{in}, mass flow rate $\dot{m}_{in}$, specific heat capacity $c_{p,in}$ as well as the electric drive efficiency η_{mot} and the isentropic efficiency η_{is}:

$$P_{el} = \frac{1}{\eta_{mot} \cdot \eta_{is}} \cdot \dot{m}_{in} c_{p,in} T_{in} \cdot \left(\left(\frac{p_{out}}{p_{in}} \right)^{\frac{\kappa-1}{\kappa}} - 1 \right). \tag{3}$$

Lastly, the required electric power for the electrolyzer is determined via the produced mass flow of hydrogen $\dot{m}_{out,H_2}$, its lower heating value $LHV(H_2)$ and the electrolysis efficiency η:

$$P_{el} = \frac{1}{\eta} \cdot \dot{m}_{out,H_2} \cdot LHV(H_2). \tag{4}$$

The reactor modeling including the interplay of its volume V (i.e. residence time) and the time dependent reduction process is addressed in more detail, subsequently.

3.2. Reactor modeling

The flash reactor is at the heart of the reduction plant and its model is therefore crucial for the analysis of the entire process. While the other components do not require a temporal resolution of the residence time, this is crucial for the adequate description of the reduction reaction taking place in the reactor. Recall the global rate equation (1) modeling the time dependent fractional reduction degree X. The considered plug flow reactor model further assumes time dependent partial pressures p_{H_2}, p_{H_2O} within the reactor to account for the impact of the proceeding reaction (i.e. change in partial pressure lead to a change in reaction rate). In the real process the required external heat is provided by partial oxidation of some hydrogen. However, in the deployed reactor model isothermal conditions are assumed, which are achieved by external heat supply. As before, let $\dot{m}_{in,s}$ denote the mass flow rate of species s at the reactor inlet and in addition let $\dot{m}_{R,s}(t)$ denote the mass flow rate of species s throughout the residence time in the reactor R and $\overline{M}_s$ the molar mass of species s. Then, the mass balances of the components considering the global reaction (R1) are described by

$$\dot{m}_{R,Fe_2O_3}(t) = (1 - X(t)) \cdot \dot{m}_{in,Fe_2O_3}, \qquad \dot{m}_{R,Fe}(t) = 2X(t) \cdot \dot{m}_{in,Fe_2O_3} \frac{\overline{M}_{Fe}}{\overline{M}_{Fe_2O_3}}, \tag{5}$$

$$\dot{m}_{R,H_2O}(t) = \dot{m}_{in,H_2O} + 3X(t) \cdot \dot{m}_{in,Fe_2O_3} \frac{\overline{M}_{H_2O}}{\overline{M}_{Fe_2O_3}}, \qquad \dot{m}_{R,H_2}(t) = \dot{m}_{in,H_2} - 3X(t) \cdot \dot{m}_{in,Fe_2O_3} \frac{\overline{M}_{H_2}}{\overline{M}_{Fe_2O_3}}. \tag{6}$$

These representations can be used to define the time dependent partial pressures

$$p_s(X(t)) = p_{in} \frac{\frac{\dot{m}_{in} x_{R,k}(t)}{\overline{M}_k}}{\frac{\dot{m}_{in} x_{R,H_2}(t)}{\overline{M}_{H_2}} + \frac{\dot{m}_{in} x_{R,H_2O}(t)}{\overline{M}_{H_2O}}}, \quad s \in \{H_2, H_2O\}. \tag{7}$$

Using (1) and (5) to (7) the reactor is modelled as follows

$$\frac{dX}{dt} = 4.41 \cdot 10^7 \cdot e^{\frac{-E_A}{R \cdot T}} \cdot \left(p_{H_2}(X(t)) - \frac{p_{H_2O}(X(t))}{K_{eq}(T(t))} \right) \cdot (1 - X(t)), \qquad X(0) = 0. \tag{8}$$

To use the presented reactor model as optimization constraints, the differential equation (8) is discretized using an implicit Euler discretization scheme with a fixed number of discretization steps N and a variable discretization step length h to represent the solution X_ℓ at time steps $t_\ell, \ell = 0, \dots, N-1$. The residence time within the reactor is thus given by t_{N-1} and has to coincide with the ratio of the reactor volume V and the volumetric flow rate $\dot{V}$, i.e. $t_{N-1} = \frac{V}{\dot{V}}$, where $\dot{V}$ is defined by the general gas law.

3.3. Economic objective function

The overall goal of industrial production is to maximize profits, which can be accomplished by either raising the product's selling price or lowering production costs. The latter is typically achieved through the analysis of marginal production costs. To this end, the levelized cost of iron (*LCOI*) serves as the economic objective function, taking into account various costs such as capital expenditures (*CAPEX*), operational expenditures (*OPEX*), energy costs (C_{el}), and transport expenses (C_{trans}), all relative to the yearly production of iron ($m_{Fe,year}$):

$$LCOI = \frac{CAPEX + OPEX + C_{el} + C_{trans}}{m_{Fe,year}}. \qquad [\$/\text{kg iron}] \tag{9}$$

Within the framework of the previously outlined iron-energy cycle (cf. Section 1.), transport costs are linked to long-distance transport costs, while the expenses associated with the feedstock (Fe_2O_3) are not taken into

consideration, as it is continuously recycled. Similarly, costs pertaining to short-distance transport and related logistics are excluded from this investigation. Additionally, it is assumed that the reduction degree of the iron has little effect on its suitability for the generation of high-temperature heat or electricity. Nevertheless, it is important to note that reducing the degree of reduction leads to an increase in the amount of material transported, resulting in higher transportation costs that are taken into account in the objective function.

3.3.1. Capital expenditures

The annuity method is a widely recognized approach for assessing projects from an economic viewpoint because of its simplicity and transparency [12]. It involves computing uniform yearly capital expenditures *CAPEX* that correspond to the present value of the initial investment expenses (*CC*), which can be determined by applying a capital recovery factor (*CRF*), i.e. a constant discount rate i over the project's economic life span n:

$$CAPEX = CRF \cdot CC = \frac{i \cdot (1+i)^n}{(1+i)^n - 1} \cdot CC. \qquad [\$/\text{year}] \tag{10}$$

3.3.2. Operational expenditures

The *OPEX* contrasts the *CAPEX* and comprises maintenance and operating costs. It is commonly provided as a fraction γ of the capital costs: According to [13], the yearly maintenance cost can be estimated to be 6% of the fixed capital cost *CC*. This yields

$$OPEX = \gamma \cdot CC. \qquad [\$/\text{year}] \tag{11}$$

3.3.3. Energy cost

The energy cost for the presented reduction plant refers to the electricity cost c_{el} assumed to come from RE sources and used for the water electrolysis, the compressors, as well as for the heat requirements of the reactor:

$$C_{el} = (P_{el}^{electrolyzer} + P_{el}^{air\ fan} + P_{el}^{recycle\ compressor} + \dot{Q}_{therm}^{reactor}) \cdot c_{el} \cdot t_{year}, \qquad [\$/\text{year}] \tag{12}$$

where P_{el}^{i} denotes the electric power of component i, $\dot{Q}_{therm}^{reactor}$ accounts for the consumed power of the reactor's external heat supply and t_{year} denotes the operation hours within one year.

3.3.4. Transport cost

As previously explained, only long-distance transport costs will be considered. Therefore, it is assumed that the yearly produced iron $m_{Fe,year}$ and the yearly remaining iron oxide $m_{Fe_2O_3,year}$ have to be transported over a long-range distance $dist_{trans}$ at a daily transport cost of $c_{trans,day}$ using n_{ships} with vessel size m_v each travelling with velocity v_{trans}. In total, this yields the following yearly transport costs:

$$C_{trans} = \frac{dist_{trans}}{v_{trans}} \cdot n_{ships} \cdot c_{trans,day} = \frac{dist_{trans}}{v_{trans}} \cdot \frac{m_{Fe,year} + m_{Fe_2O_3,year}}{m_v} \cdot c_{trans,day}. \qquad [\$/\text{year}] \tag{13}$$

3.3.5. Fixed capital cost

The fixed investment costs are based on the cost for the major equipment used in the process (i.e. within the given flow diagram in Fig. 2), which is a common way to derive appropriate estimates in early stages of process synthesis [13, 14]. The cost of each module is determined in dependence of the module size, i.e. the design variables introduced in Section 3.1. The estimated capital cost then results in the sum over all estimated equipment costs. The different components of the capital cost are briefly summarized in the following, for further details please refer to [13].

Costs are commonly represented as power law of capacity, i.e. the equipment cost C_E with capacity Q_E is given by $C_E = C_B\left(\frac{Q_E}{Q_B}\right)^M$, with known base costs C_B of the equipment with base capacity Q_B and an equipment dependent constant M.

Furthermore, the validity of economic data is highly dependent on the publishing date and therefore requires normalization to a common basis which can be done by the means of cost indices (e.g. Chemical Engineering Plant Cost Index (CEPCI) [15]). To account for different materials, design pressures, and temperatures, additional correction factors are used to determine the purchase costs of equipment. These factors include f_M for materials, f_p for design pressure, and f_T for design temperature. In addition, piping costs are accounted for with the factor f_{PIP}, while other direct costs, such as equipment erection and instrumentation, and indirect costs, including engineering and construction, as well as working capital are considered in the total cost calculation with the factor f_{misc}. This leads to the following representation of the fixed capital costs:

$$CC = \sum_j \left(\left(f_M f_p f_T (1 + f_{PIP}) \right)_j + f_{misc} \right) \frac{CEPCI_{year}}{CEPCI_{reference\ year}} C_{B,j} \left(\frac{Q_{E,j}}{Q_{B,j}} \right)^M. \qquad [\$] \tag{14}$$

https://doi.org/10.52202/069564-0117

3.4. Properties and assumptions

Modern ironmaking plants produce between 0.3 Mio and 3 Mio tons of iron per year [7]. Therefore, it is assumed that the continuous Fe_2O_3 feed into the reduction plant amounts 50 kg s^{-1}, leading to 34.97 kg s^{-1} of produced iron when assuming a fractional reduction degree of $X = 1$ and thus to 0.99 Mio tons/year when assuming 328 continuous operating days of the reduction plant and to 1.06 Mio tons/year when assuming 350 continuous operating days.
In the following, several properties and assumptions used in the model definition are summarized. Note that in the computation of numerical results (cf. Section 4.) for properties characterized by feasible ranges, as long as not stated otherwise, the mean value of the range is considered.
Thermodynamic properties such as molar masses are taken from [16]. In order to avoid an increase in the model complexity by modelling discontinuous piecewise polynomial representations for the temperature dependent enthalpy using NASA Glenn coefficients [16], a linear approximation for the enthalpy is computed and used to determine temperature independent constant specific heat capacity values.
When analyzing the numerical results, besides the already presented metrics also the energetic efficiency of the considered system will be assessed. This metric is defined by

$$\eta_{sys} = \frac{HV(Fe) \cdot \dot{m}_{Fe}}{(P_{el}^{electrolyzer} + P_{el}^{air\ fan} + P_{el}^{recycle\ compressor} + \dot{Q}_{therm}^{reactor})}, \tag{15}$$

i.e. the ratio of the energy stored in iron (given by the product of the heating value $HV(Fe)$ of iron and the produced mass flow rate of iron $\dot{m}_{Fe}$) and the total energy supplied to the process as defined in (12).

Table 2: General economic and transport assumptions

Variable	Value/Range	Reference
OPEX fraction γ of *CC*	6%	[13]
Interest rate i	5–8 %	[17]
Economic life time n	20–25 years	[17]
Price for RE c_{el}	0.01–0.10 \$/kWh	[18]
Operational days	328–350 days	[17]
Transport distance	3000–20 000 km	Assumption
Vessel size	160 000 t	[5]
Daily transport costs	5000–50 000 \$/day	[19]
Transport speed	624 km/day	[5]

3.4.1. Technological assumptions

Heat Exchangers
It is assumed that any heat loss originating from other components than the reactor is associated to the heat exchangers, i.e. the air heater, the iron oxide preheater, the hydrogen preheater and the condenser. It is estimated that between 1–5 % of the transferred heat will be lost to the environment instead of being transferred to the cold medium. Further assumptions concerning the heat exchangers are summarized in Table 3.
Cyclone
By assumption, all of the hot reduced iron is separated from the gaseous residual stream within the cyclone. While the cyclone is not specifically designed and optimized for this process, values from a high loaded hot gas cyclone given in [11] are used. Based on this design, the pressure drop is expected to be within the range of $\Delta p = 0.1 - 0.2$ bar.
Electrolyzer
The system efficiency based on the lower heating value of the electrolysis is predicted to be in the range of 50-74 % according to IEA and IRENA [20, 21]. In this use case an efficiency of $\eta = 71\%$ is assumed.
Compressors
For the air fan and the recycle compressor an isentropic efficiency of $\eta_{is} = 85\%$ and an electrical drive efficiency of $\eta_{mot} = 95\%$ is assumed. The heat capacity ratio κ as in (3) is assumed to be $\kappa = 1.4$ for both, the air compressor and the hydrogen recycle compressor.

Table 3: Heat exchanger assumptions including type, pressure drop Δp and heat transfer coefficient U

Component	Type	Δp [bar]	U [W m^{-2} K^{-1}]	References
Iron Oxide Preheater Air Heater	Bulk solid heat exchanger	0.14	100-144	[22–25]
Hydrogen Preheater	Alternating regenerators	0.14	6	[11]
Condenser	Tube and shell	0.05	300-1200	Assumption / [11, 22]

https://doi.org/10.52202/069564-0117

3.4.2. Economic assumptions

As presented in Section 3.3.5. the fixed capital cost includes several correction factors and economic indices for cost normalization. The correction factors are chosen according to [13] and take the following values. For all components except for the electrolyzer the material correction factor f_M is assumed to be $f_M = 3.4$ (high grade stainless steel), the pressure correction $f_p = 1.0$, the piping correction factor $f_{PIP} = 0.7$ and the remaining factors are summarized in $f_{misc} = 5.1$. The electrolyzer and associated periphery costs are directly taken from the literature. Consequently, the correction factors are set to $f_M = f_p = f_{PIP} = 1.0$ and $f_{misc} = 0$. In order to account for potential high process temperatures, a correction factor for temperature is extrapolated based on values given in [13]: $f_T = \max(1,\ 2.75\,^\circ\mathrm{C} \cdot 10^{-3} \cdot T_{max} + 0.742)$ with T_{max} denoting the maximum process temperature for each component. The costs are normalized to the year 2021 using the CEPCI of 708.0 [15]. All base costs, base capacities, reference years and indices can be found in Table 4. According to [20, 21] the electrolyzer capital cost can be estimated to be in the range of 450-1400$\,\$/\mathrm{kW}$ multiplied by the electric power.

Table 4: Capital costs of equipment; the hydrogen preheater costs are based on [26], the cost of the electrolyzer is estimated based on [20, 21] and the cost functions of all other components are based on [13]

Component	Ref. year /CEPCI	$C_{B,j}$[\$]	$Q_{B,j}$	M	$C_{E,j}$
Iron Oxide Preheater Air Heater Condenser	2000 / 391.1	$3.28 \cdot 10^4$	80 m^2	0.68	
Air compressor Recycle Compressor	2000 / 391.1	$9.84 \cdot 10^4$	0.25 MW	0.46	$\frac{CEPCI_{2021}}{CEPCI_{reference\ year}} C_{B,j} \left(\frac{Q_{E,j}}{Q_{B,j}}\right)^M$
Reactor	2000 / 391.1	$1.15 \cdot 10^4$	5 m^3	0.53	
Hydrogen Preheater	1981 / 297.0	$0.85 \cdot 10^6$	6555 m^2	0.6	
Electrolysis	–	–	–	–	$925\,\$/\mathrm{kW_{el}} \cdot P_{el}$

4. Numerical results and discussion

The presented techno-economical model with the introduced *LCOI* (cf. (9)) as objective is optimized using mathematical optimization algorithms in order to obtain the optimal process design and operation of the reduction plant for varying economic assumptions (i.e. price for RE, *CRF*). Given the significant variation in RE prices depending on the location and type of renewable energy plant [18], and the sensitivity of annualized capital costs to the *CRF* - and consequently to the assumed interest rate and economic lifetime - the impact of these economic constraints on the *LCOI* and the resulting optimized plant designs is evaluated. It should be noted that the *LCOI* is primarily influenced by the total capital cost (*CC*) in terms of both capital expenditure (*CAPEX*) and operating expenditure (*OPEX*), as well as the yearly energy consumption in terms of C_{el}. Additionally, the transportation costs (C_{trans}) and annual iron production ($m_{Fe,year}$) are indirectly impacted by the yearly energy consumption, as the energy consumed during the electrolysis process determines the quantity of produced iron, which subsequently affects the mass fractions of unreduced iron oxide and produced iron, ultimately influencing the transportation costs. Therefore, it is expected that the solutions, obtained by minimizing the *LCOI*, represent trade-offs between the yearly energy consumption and the total capital cost. To investigate and quantify this trade-off, the optimization is performed multiple times with varying values for c_{el} and *CRF* weighting the yearly energy consumption and the total capital costs in the objective function.
The resulting optimization problem is implemented using PySCIPOpt [27], an interface to the mixed-integer nonlinear problem solver SCIP [28], relying on a spatial branch-and-bound algorithm.
Although SCIP is able to perform global optimization, the following results could not be certified to be global solutions within reasonable time due to the complexity of the model characterized by nonlinear model equations as well as the discretized ODE constraint presented in Section 3.2. The solutions are obtained by a local NLP solver used as heuristic in the SCIP framework and therefore constitute local optimal solutions.

4.1. Fixed CRF and varying energy costs

In a first step, the optimization problem is solved for varying energy costs $c_{el} \in \{0, 10, 55, 70, 100, 150, 200\}$ [\$/MWh] with a fixed $CRF \approx 0.085$, i.e. assuming an economic life time of $n = 23$ years and an interest rate of $i = 6.5\%$. The obtained objective values and the corresponding shares of *CAPEX*, *OPEX*, energy and transport costs are depicted in Fig. 3. The resulting *LCOI* varies between $0.05\,\$/\mathrm{kg}$ iron and $0.68\,\$/\mathrm{kg}$ iron. As to be expected there is a close to linear relation between the energy price and the resulting *LCOI*. The variance in the *LCOI* showcases the high dependency of the competitiveness of the investigated process on suitable locations with low prices for RE. The figure also shows that the transportation costs play an insignificant role for the *LCOI*. This suggests, that it could be beneficial to choose reduction locations with rather high transport distances if in return RE is available at low prices. The results further show that at high prices for RE (e.g.

https://doi.org/10.52202/069564-0117

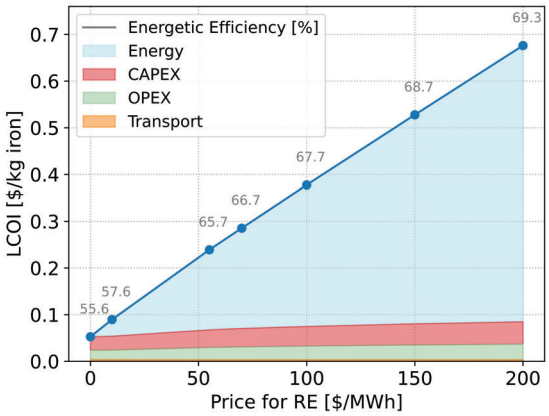

Figure 3: Objective values obtained by minimizing the *LCOI* with a fixed *CRF* ≈ 0.085 and varying values for the energy cost c_{el} of RE

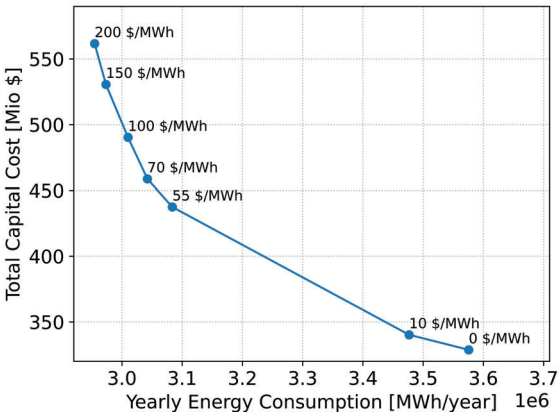

Figure 4: Yearly energy consumption versus total capital cost at the optimization solutions for fixed *CRF* and varying values for c_{el}

200 $/MWh), energy costs are dominant, accounting for a significant percentage (87.5%) of the *LCOI*. In contrast, at low energy prices (e.g. 10 $/MWh), a balance is observable between energy and equipment-related costs, with energy costs contributing 39.8% to the *LCOI*. Additionally, with increasing cost for RE, also the energetic efficiency of the system increases from η_{sys} = 55.6% to η_{sys} = 69.3%. For further analyses Fig. 4 shows the relationship between the yearly energy consumption and the total capital cost for the different values of c_{el}. The results indicate that as the price for RE increases, process designs with lower energy demands (and therefore higher energetic efficiencies), but higher total capital costs (due to larger component dimensions) are economically more advantageous. This suggests that an optimal design of the considered reduction plant represents a trade-off between the yearly energy consumption and the total investment costs and is highly dependent on the cost assumptions for RE.

The optimal design variables illustrate the described behaviour. With increasing c_{el} the reactor volume increases from 1574 to 5519 m^3 and the fractional reduction degree X increases from 94.6% to 97.6%, while the reactor temperature remains constant at 1423 K and the hydrogen equivalence ratio λ_{H_2} only varies slightly between 2.55 and 2.32. The increase in the reduction degree is directly related to an increase in the required electrical power $P_{el}^{electrolyzer}$ of the electrolyzer. The condenser area shows an increase from $0.73 \cdot 10^3$ to $1.53 \cdot 10^3$ m^2, the air preheater area an increase from $0.03 \cdot 10^3$ to $3.56 \cdot 10^3$ m^2 and especially the hydrogen preheater an increase from $1.53 \cdot 10^3$ to $55.4 \cdot 10^3$ m^2. The increasing dimensions of the design variables account for the higher total capital cost with increasing RE prices. Regarding the yearly energy consumption, the values for the recycle compressor and the air compressor only vary little, and the yearly energy consumption of the electrolyzer increases from 2.46 to 2.54 TWh due to the increasing reduction degree as explained before. However, the yearly energy consumption of the external heat supply for the reactor decreases from 1.1 to 0.4 TWh. This leads to the overall decreasing yearly energy consumption for increasing RE prices.

Upon examining the shares of the total capital cost of each component, as depicted in Fig. 5, it can be noted that in a scenario where RE is free of charge, the electrolyzer comprises over 80% of the investment cost. As the cost of RE increases, the proportion of investment cost attributed to the electrolyzer declines, yet it still constitutes over 50% of the investment cost at the highest considered cost for RE. Furthermore, the electrolyzer is responsible for nearly 70% of the yearly energy consumption with c_{el} = 0 $/MWh and for more than 85% with c_{el} = 200 $/MWh. Considering that the electrolyzer incurs substantial capital costs and energy demand, it has the highest potential for reducing energy demand, capital costs, and consequently the *LCOI* through technological improvements.

Although the costs for turbo-machinery are negligible, the cost shares of the heat recovery equipment, including the air heater, the iron oxide preheater, and the hydrogen preheater experience a significant increase with increasing costs of RE. As the sizes of the associated heat exchangers increase, along with their corresponding costs, a greater amount of the available sensible heat within the reactor effluents can be recovered, resulting in decreased energy dissipation in the condenser and lower residual energy within exiting streams. Ultimately this leads to a reduced energy demand of the reactor. Especially the regenerative hydrogen preheater plays a crucial role for the heat recovery and the reduced energy demand, which is reflected by its increasing share of the capital costs for higher energy costs.

https://doi.org/10.52202/069564-0117

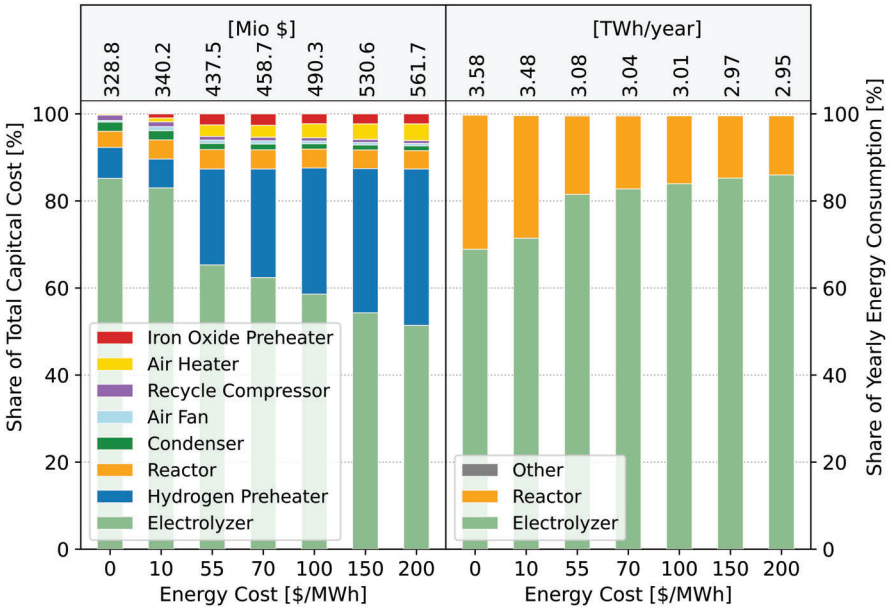

Figure 5: Components' shares of the total capital cost and the yearly energy consumption at the optimization solutions for fixed *CRF* and varying values for c_{el}.

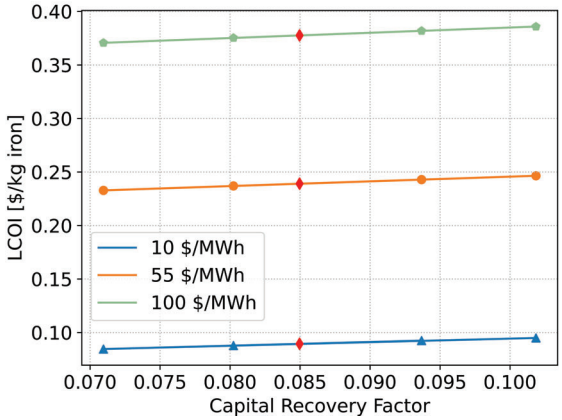

Figure 6: Objective values obtained by minimizing the *LCOI* with varying values for *CRF* $\in \{0.071, 0.080, 0.094, 0.102\}$ and $c_{el} \in \{10, 55, 100\}$ [$/MWh]; red diamonds represent base *CRF* (n = 23 years, i = 6.5%)

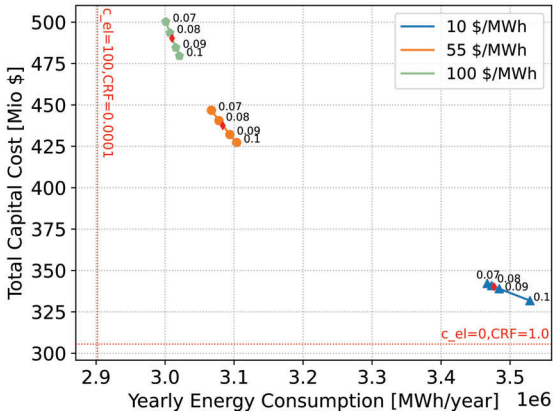

Figure 7: Yearly energy cost versus total capital cost at the optimal solutions for varying values of *CRF* and c_{el}; red diamonds represent base *CRF* (n = 23 years, i = 6.5%); lower bounds obtained by optimization with the specified parameters

4.2. Varying CRF and varying energy costs

As mentioned earlier, the impact of capital costs on the *LCOI* is significant at low to moderate prices for RE. However, the annualized capital costs demonstrate high sensitivity to the assumed *CRF*, and thus, to the assumed interest rate and economic lifetime. To address this uncertainty, the optimization problem was solved for varying energy costs $c_{el} \in \{10, 55, 100\}$ [$/MWh] and varying values for *CRF* $\in \{0.071, 0.080, 0.094, 0.102\}$ corresponding to economic life times of n = 20 and n = 25 years and interest rates of i = 5 and i = 8%. Figure 6 shows the obtained objective values for the different RE costs in dependence of the *CRF* values together with the *LCOI* for the base case (n = 23 years, i = 6.5%, red diamonds) considered in the previous section. Again

https://doi.org/10.52202/069564-0117

an expected nearly linear relation and a clear shift depending on the energy cost is observable. For c_{el} = 10 \$/MWh, the *LCOI* depending on the *CRF* varies between 0.085 \$/kg iron (-5.5% compared to base *CRF*) and 0.095 \$/kg iron (+6.1% compared to base *CRF*), for c_{el} = 55 \$/MWh between 0.233 \$/kg iron (-2.6%) and 0.246 \$/kg iron (+3.1%) and for c_{el} = 100 \$/MWh between 0.371 \$/kg iron (-1.8%) and 0.386 \$/kg iron (+2.2%) demonstrating the sensitivities of the *LCOI* depending on c_{el} and *CRF*. The results show that the relative impact of the *CRF* assumptions increases for low RE prices.
In addition, the total capital cost is plotted against the yearly energy consumption in Fig. 7 for the varying values of *CRF* and c_{el}. It can be seen, that the total capital cost decreases with increasing values of *CRF* and decreasing values of c_{el}, whereas the yearly energy consumption increases with increasing values of *CRF* and decreasing values of c_{el}. This again indicates the trade-off between the total investment costs and the yearly energy consumption mentioned before. The red lines show the lower bounds for the total capital cost and the yearly energy consumption. On the one hand, the lower bound for the capital cost is obtained by solving the optimization problem with c_{el} = 0 and *CRF* = 1.0, resulting in *CC* = 305.6 Mio \$/year. On the other hand, the lower bound for the yearly energy consumption is obtained by solving the optimization problem with c_{el} = 100, *CRF* = 0.0001 and γ = 0.0 (*OPEX* fraction of *CC*), resulting in a yearly energy consumption of 2.9 TWh/year. These extreme cases result in energetic efficiencies of η_{sys} = 71.6% for high c_{el} and low *CRF* and η_{sys} = 55.4% for low c_{el} and high *CRF* underlining the strong dependence of the optimal process design on the economic boundary conditions and showing the techno-economic limits (highest achievable efficiency vs. lowest achievable capital cost) for the investigated reduction plant.

5. Conclusion and outlook

This work has presented a techno-economic analysis of an innovative reduction plant, based on the flash ironmaking technology, that could be part of a circular energy economy allowing the large-scale storage and transport of RE using iron as energy carrier. The assessment was performed with the goal of investigating the influence of changing economic boundary conditions (price for RE, *CRF*) on the economically optimal process design.
Based on the performed analyses, it can be concluded that the price for RE has a significant impact on the *LCOI*. The resulting *LCOI* varies between 0.05 \$/kg iron and 0.68 \$/kg iron for energy costs between 0 \$/MWh and 200 \$/MWh, respectively. The investigation reveals that changing RE prices lead to noteworthy differences in design parameters such as component dimensions. As the cost of RE rises, effective heat recovery becomes increasingly important with respect to the *LCOI*, resulting in higher capital costs due to larger equipment, but lower energy demands and higher energetic efficiencies (η_{sys} = 55.6% to η_{sys} = 69.3%). In addition, the results emphasize that access to low-cost RE can offset the expenses linked with long-distance transportation. Since RE costs outweigh transport costs, it can be inferred that selecting appropriate reduction sites with access to affordable RE is crucial. Varying *CRF* values (i.e. economic lifetime and interest rate) further reinforce the trade-off between total capital costs and yearly energy consumption, even though the influence of the considered *CRF* values is less prominent than the change in RE prices. Yet, for lower RE prices, the relative effect of changing *CRF* assumptions increases.
Throughout the analysis, the reduction plant was assumed to operate continuously for a fixed number of operating days, assuming continuous availability of RE. However, due to the volatile nature of RE availability, intermediate storage options for green hydrogen and/or RE are necessary to ensure the continuous operation of the reduction plant. In future work, the model will be expanded to integrate such storage options and to couple the reduction plant model with models for RE systems, such as photovoltaic and wind power plants. This would enable the optimization of the entire storage process for the iron energy cycle and result in location specific optimal designs, based on different geographic locations and their RE potential. Additionally, considering uncertainties, e.g. fluctuations in the price or availability of RE, and applying robust optimization strategies to obtain robust process designs, would be a valuable direction for future research.

Acknowledgements

Funding by the Hessian Ministry of Higher Education, Research, Science and the Arts - cluster project Clean Circles is gratefully acknowledged.

Nomenclature

A	area, m^2	$\overline{M}$	molar mass, $kg\,kmol^{-1}$
C	cost, \$	$\dot{m}$	mass flow rate, $kg\,s^{-1}$
c_p	specific heat capacity, $J\,kg^{-1}\,K^{-1}$	p	pressure, bar
E_A	activation energy, $J\,mol^{-1}$	P_{el}	electric power, W

Q capacity,

$\dot{Q}_{therm}$ heat flow, W

R universal gas constant, $\mathrm{J\,kg^{-1}\,K^{-1}}$

T temperature, K

t time, s

U heat transfer coefficient, $\mathrm{W\,m^{-2}\,K^{-1}}$

V volume, $\mathrm{m^3}$

$\dot{V}$ volumetric flow rate, $\mathrm{m^3\,s^{-1}}$

Greek symbols

γ *OPEX* fraction of *CC*

Δ difference

η energetic efficiency

κ heat capacity ratio

λ hydrogen equivalence ratio

Subscripts and superscripts

B base

E equipment

el electrical

eq equilibrium

in incoming

is isentropic

M material

max maximum

min minimum

misc miscellaneous

mot motor

out outgoing

p pressure

PIP piping

R reactor

s species

sys system

T temperature

therm thermal

trans transport

v vessel

References

[1] IEA. *Renewables 2022*. URL: https://www.iea.org/news/renewable-power-s-growth-is-being-turbocharged-as-countries-seek-to-strengthen-energy-security (visited on Jan. 24, 2023).

[2] Bergthorson J. M. *Recyclable metal fuels for clean and compact zero-carbon power*. In: Progress in Energy and Combustion Science 68 (2018), pp. 169–196. DOI: 10.1016/j.pecs.2018.05.001.

[3] Dirven L., Deen N. G., and Golombok M. *Dense energy carrier assessment of four combustible metal powders*. In: Sustainable Energy Technologies and Assessments 30 (2018), pp. 52–58. DOI: 10.1016/j.seta.2018.09.003.

[4] Debiagi P. et al. *Iron as a sustainable chemical carrier of renewable energy: Analysis of opportunities and challenges for retrofitting coal-fired power plants*. In: Renewable and Sustainable Energy Reviews 165 (2022), p. 112579. DOI: 10.1016/j.rser.2022.112579.

[5] Neumann, J. and da Rocha, R. C. et al. *Techno-economic assessment of long-distance supply chains of energy carriers: Comparing hydrogen and iron for carbon-free electricity generation*. In: Applications in Energy and Combustion Science 14 (2023), p. 100128. DOI: 10.1016/j.jaecs.2023.100128.

[6] Janicka J. et al. *The potential of retrofitting existing coal power plants: a case study for operation with green iron*. In: Applied Energy (2023). DOI: 10.1016/j.apenergy.2023.120950.

[7] Sohn H. Y., Fan D.-Q., and Abdelghany A. *Design of Novel Flash Ironmaking Reactors for Greatly Reduced Energy Consumption and CO2 Emissions*. In: Metals 11.2 (2021), p. 332. DOI: 10.3390/met11020332.

[8] Chen F. et al. *Hydrogen Reduction Kinetics of Hematite Concentrate Particles Relevant to a Novel Flash Ironmaking Process*. In: Metallurgical and Materials Transactions B 46.3 (2015), pp. 1133–1145. ISSN: 1073-5615. DOI: 10.1007/s11663-015-0332-z.

[9] Sohn H. Y. *Energy Consumption and CO2 Emissions in Ironmaking and Development of a Novel Flash Technology*. In: Metals 10.1 (2020), p. 54. DOI: 10.3390/met10010054.

[10] Spreitzer D. and Schenk J. *Reduction of Iron Oxides with Hydrogen—A Review*. In: steel research international 90.10 (2019), p. 1900108. ISSN: 1611-3683. DOI: 10.1002/srin.201900108.

https://doi.org/10.52202/069564-0117

[11] *VDI heat atlas*. 2nd ed. VDI-buch. Berlin and New York: Springer, 2010. ISBN: 9783540778769.

[12] Bejan A., Tsatsaronis G., and Moran M. J. *Thermal design and optimization*. New York and Chichester: John Wiley, 1996. ISBN: 0471584673.

[13] Smith R. *Chemical process design and integration*. Second edition. Chichester West Sussex United Kingdom: Wiley, 2016. ISBN: 9781119990147.

[14] Turton R. *Analysis, synthesis, and design of chemical processes*. 3rd ed. Prentice Hall PTR international series in the physical and chemical engineering sciences. Upper Saddle River N.J.: Prentice Hall, 2009. ISBN: 0135129664.

[15] Chemical Engineering. *The Chemical Engineering Plant Cost Index - Chemical Engineering*. 2023. URL: https://www.chemengonline.com/pci-home (visited on Feb. 22, 2023).

[16] McBride B. J., Zehe M. J., and Gordon S. *NASA Glenn Coefficients for Calculating Thermodynamic Properties of Individual Species*. 2002. URL: https://ntrs.nasa.gov/citations/20020085330 (visited on Feb. 22, 2022).

[17] International Energy Agency. *Iron and steel technology roadmap: Towards more sustainable steelmaking*. Energy technology perspectives series. [Paris, France]: IEA Publicatons, 2020. ISBN: 9789264441149. URL: https://iea.blob.core.windows.net/assets/eb0c8ec1-3665-4959-97d0-187ceca189a8/Iron_and_Steel_Technology_Roadmap.pdf (visited on Feb. 21, 2023).

[18] International Renewable Energy Agency. *Renewable power generation costs in 2021*. URL: https://www.irena.org/-/media/Files/IRENA/Agency/Publication/2022/Jul/IRENA_Power_Generation_Costs_2021.pdf?rev=34c22a4b244d434da0accde7de7c73d8 (visited on Feb. 22, 2023).

[19] BIMCO. *Dry bulk - profits surge to multi-year highs as pandemic related demand and disruptions linger*. 2021. URL: https://www.bimco.org/news/market_analysis/2021/20210903-dry-bulk---profits-surge-to-multi-year-highs-as-pandemic-related-demand-and-disruptions-linger (visited on Feb. 22, 2023).

[20] International Energy Agency - IEA. *The Future of Hydrogen: Seizing todays opportunities*. 2019. URL: https://iea.blob.core.windows.net/assets/9e3a3493-b9a6-4b7d-b499-7ca48e357561/The_Future_of_Hydrogen.pdf (visited on Feb. 20, 2023).

[21] The International Renewable Energy Agency. *Green hydrogen cost reduction: Scaling up electrolysers to meet the 1.5C climate goal*. 2020. URL: https://irena.org/-/media/Files/IRENA/Agency/Publication/2020/Dec/IRENA_Green_hydrogen_cost_2020.pdf (visited on June 14, 2021).

[22] Albrecht K. J. and Ho C. K. *Heat Transfer Models of Moving Packed-Bed Particle-to-SCO2 Heat Exchangers*. In: *ASME 2017 11th International Conference on Energy Sustainability*. American Society of Mechanical Engineers, 2017. ISBN: 978-0-7918-5759-5. DOI: 10.1115/ES2017-3377.

[23] Saleh N. S. et al. *Experimental Investigation of a Moving Packed-Bed Heat Exchanger Suitable for Concentrating Solar Power Applications*. In: Applied Sciences 12.8 (2022), p. 4055. DOI: 10.3390/app12084055.

[24] Solex Thermal Sciences. *Solex Thermal Sciences — Energy Efficient Heat Exchanger Technology*. 2023. URL: https://www.solexthermal.com/our-technology/ (visited on Feb. 18, 2023).

[25] John E. Edwards. *Design and Rating of Shell and Tube Heat Exchangers*. 2008. URL: http://www.citwulkow.chemstations.com/content/documents/Technical_Articles/shell.pdf (visited on Feb. 20, 2023).

[26] Dastur Engineering International GMBH. *Report on Evaluation of Tender for the Valentine Iron Ore Project in Uruguay*. 1981. URL: https://inis.iaea.org/collection/NCLCollectionStore/_Public/41/076/41076189.pdf (visited on Feb. 20, 2023).

[27] Maher S. et al. *PySCIPOpt: Mathematical Programming in Python with the SCIP Optimization Suite*. In: *Mathematical Software – ICMS 2016*. Springer International Publishing, 2016, pp. 301–307. DOI: 10.1007/978-3-319-42432-3_37.

[28] Bestuzheva K. et al. *The SCIP Optimization Suite 8.0*. ZIB-Report 21-41. Zuse Institute Berlin, Dec. 2021. URL: http://nbn-resolving.de/urn:nbn:de:0297-zib-85309.